Title

RNA binding protein DDX5 restricts RORγt+ Treg suppressor function to promote intestine inflammation

Journal

Science Advances, 9(5)

ISSN

2375-2548

Authors

Ma, Shengyun

Yang, Qiyuan

Chen, Nicholas

et al.

Publication Date

2023-02-03

DOI

10.1126/sciadv.add6165

IMMUNOLOGY

RNA binding protein DDX5 restricts RORγt$^+$ T$_{reg}$ suppressor function to promote intestine inflammation

Shengyun Ma[1]*, Qiyuan Yang[2], Nicholas Chen[1], Anna Zheng[1], Nazia Abbasi[1], Gaowei Wang[3], Parth R. Patel[1]†, Benjamin S. Cho[1], Brian A. Yee[1], Lunfeng Zhang[4], Hiutung Chu[5,6], Sylvia M. Evans[4,7,8], Gene W. Yeo[1], Ye Zheng[2], Wendy Jia Men Huang[1]*

Retinoid-related orphan receptor (RAR) gamma (RORγt)–expressing regulatory T cells (RORγt$^+$ T$_{regs}$) play pivotal roles in preventing T cell hyperactivation and maintaining tissue homeostasis, in part by secreting the anti-inflammation cytokine interleukin-10 (IL-10). Here, we report that hypoxia-induced factor 1α (HIF1α) is the master transcription factor for *Il10* in RORγt$^+$ T$_{regs}$. This critical anti-inflammatory pathway is negatively regulated by an RNA binding protein DEAD box helicase 5 (DDX5). As a transcriptional corepressor, DDX5 restricts the expression of HIF1α and its downstream target gene *Il10* in RORγt$^+$ T$_{regs}$. T cell–specific *Ddx5* knockout (DDX5$^{\Delta T}$) mice have augmented RORγt$^+$ T$_{reg}$ suppressor activities and are better protected from intestinal inflammation. Genetic ablation or pharmacologic inhibition of HIF1α restores enteropathy susceptibility in DDX5$^{\Delta T}$ mice. The DDX5–HIF1α–IL-10 pathway is conserved in mice and humans. These findings reveal potential therapeutic targets for intestinal inflammatory diseases.

INTRODUCTION

Regulatory T (T$_{reg}$) cells are critical for restricting immune responses and local inflammation by limiting antigen-presenting cell activities, cytokine sequestration, cytolysis, and releasing inhibitory cytokines, including interleukin-10 (IL-10) (*1*). They express the lineage-specific transcription factor Foxp3, and recent studies also identified a role of tissue hypoxia and the hypoxia-induced factor 1α (HIF1α) in regulating their differentiation and suppressor activities in the lymph node and spleen (*2*–*7*). However, the contribution of HIF1α to intestinal T$_{reg}$ heterogeneity and suppressor functions during inflammation remains elusive. Intestinal T$_{regs}$ can be divided into two major subsets, including the conventional T$_{reg}$ (cT$_{reg}$) and RAR-related orphan receptor gamma T–expressing T$_{reg}$ (RORγt$^+$ T$_{reg}$) cells. They serve protective roles in the 2,4,6-trinitrobenzenesulfonic acid (TNBS) and T cell transfer colitis models (*8*–*10*). However, little is known about the common and/or subset-specific pathways regulating their functions in vivo.

The Asp-Glu-Ala-Asp (DEAD)–box RNA helicase DDX5 is one of the highest expressed RNA binding proteins in the intestine epithelium and is ubiquitously expressed in all T cell types (*11*, *12*). DDX5 contributes to RNA processing, mRNA export, ribosome assembly, translation, and RNA decay (*13*). Emerging evidence also suggests that DDX5 can serve as transcription coactivator and/or corepressor to regulate transcription initiation (*14*–*17*) and termination (*18*–*24*). Its expression is dysregulated in human intestine tumors and inflamed intestine lesions from inflammatory bowel diseases patients and mouse models of epithelial injury (*12*, *25*). Our recent study found that DDX5 in intestinal epithelial cells can protect against immune-mediated enteropathies (*12*, *25*). However, little is known about the role of DDX5 in the intestinal T$_{reg}$ differentiation and function under homeostatic and inflamed settings.

In this study, we report that DDX5 is a negative regulator of RORγt$^+$ T$_{reg}$ suppressor activities. Loss of DDX5 unleashes IL-10 production potential and suppressor activity in RORγt$^+$ T$_{reg}$ and protects against weight loss and pathology in two murine models of T cell–mediated intestinal inflammation. Mechanistically, DDX5 resolves the chromatin R loops on the *Hif1a* locus to restrict the expression of HIF1α and its downstream target IL-10. The DDX5–HIF1α–IL-10 pathway is evolutionarily conserved and provide potential therapeutic targets for treating T cell–mediated intestinal inflammatory diseases in humans.

RESULTS

DDX5 regulates homeostatic CD4$^+$ T cell heterogeneity and their cytokine production capacity in the intestinal lamina propria

In the steady-state small intestine and colon, DDX5 was highly expressed in the epithelial cells and the lamina propria immune cells (Fig. 1A), including T helper 17 (T$_H$17) (RORγt$^+$Foxp3$^-$), conventional Treg (cT$_{reg}$) (RORγt$^-$Foxp3$^+$), and RORγt$^+$ T$_{reg}$ (RORγt$^+$Foxp3$^+$) (Fig. 1, B to D, and fig. S1A). To explore the function of DDX5 in T lymphocytes and its contribution to intestine homeostasis and inflammation, we generated the T cell–specific *Ddx5* knockout mice (*Ddx5*$^{fl/fl}$ *Cd4*^{Cre}, annotated as DDX5$^{\Delta T}$). Control (*Ddx5*$^{+/+}$ or *Ddx5*$^{fl/+}$ *Cd4*^{Cre}, annotated as CTL) and DDX5$^{\Delta T}$ littermates were born in the Mendelian ratio. CTL and DDX5$^{\Delta T}$ mice harbored similar proportions of RORγt$^+$ T$_{reg}$,

[1]Department of Cellular and Molecular Medicine, University of California San Diego, La Jolla, CA, USA. [2]NOMIS Center for Immunobiology and Microbial Pathogenesis, Salk Institute for Biological Studies, La Jolla, CA, USA. [3]Department of Medicine, University of California San Diego, La Jolla, CA, USA. [4]Department of Pediatrics, Pediatric Diabetes Research Center, University of California San Diego, La Jolla, CA, USA. [5]Department of Pathology, University of California San Diego, La Jolla, CA, USA. [6]Chiba University–UC San Diego Center for Mucosal Immunology, Allergy, and Vaccines (cMAV), University of California San Diego, La Jolla, CA, USA. [7]Department of Pharmacology, University of California San Diego, La Jolla, CA, USA. [8]Skaggs School of Pharmacy and Pharmaceutical Sciences, University of California San Diego, La Jolla, CA, USA.
*Corresponding author. Email: zjumshy@gmail.com (S.M.); wendyjmhuang@health.ucsd.edu (W.J.M.H.)
†Present address: Western University of Health Sciences, College of Osteopathic Medicine of the Pacific, 309 E 2nd St, Pomona, CA 91766, USA.

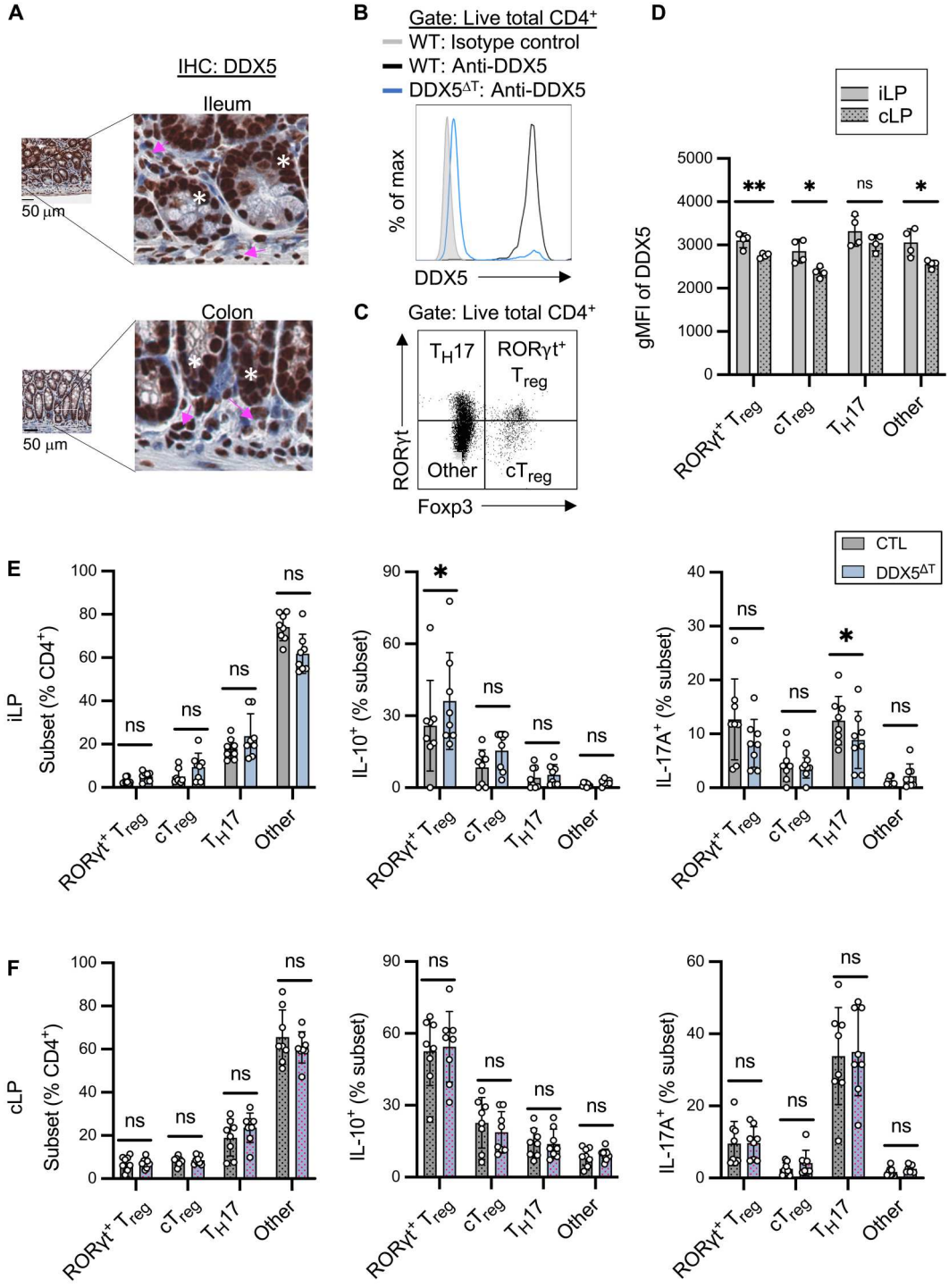

Fig. 1. DDX5 regulates homeostatic CD4$^+$ T cell heterogeneity and cytokine production capacity in the intestine lamina propria. (**A**) Representative images from immunohistochemistry analysis of DDX5 in the ileum and colon of wild-type (WT) mice. Enlarged images are shown on the right. White stars: intestinal epithelial cells; magenta arrows: intestinal infiltrated immune cells. IHC, immunohistochemistry. (**B**) Representative histogram of DDX5 protein expression in CD4$^+$ T cells from the ileal lamina propria (iLP). (**C**) Representative flow cytometry analysis of total live CD4$^+$ T cells. Gating strategy for RORγt$^+$ T_{reg} (RORγt$^+$Foxp3$^+$), cT_{reg} (RORγt$^-$Foxp3$^+$), T_H17 (RORγt$^+$Foxp3$^-$), and other (RORγt$^-$Foxp3$^-$) cells in the iLP from wild-type mice under steady state. (**D**) Geometric mean fluorescence intensity (gMFI) of DDX5 in RORγt$^+$ T_{reg}, cT_{reg}, and T_H17 from iLP and colonic lamina propria (cLP). Each dot represents the result from one mouse. *P < 0.05 and **P < 0.01; ns, not significant (multiple paired t test, n = 4). (**E**) Proportions of the indicated subsets among CD4$^+$ T cells and their IL-10 and IL-17A production potential in iLP from steady-state CTL and DDX5$^{\Delta T}$ littermates. Each dot represents the result from one mouse. (**F**) Proportions of the indicated subsets among CD4$^+$ T cells and their IL-10 and IL-17A production potential in cLP from steady-state CTL and DDX5$^{\Delta T}$ littermates. Each dot represents the result from one mouse. *P < 0.05 (multiple paired t test, n = 8).

cT_{reg}, and T_H17 (Fig. 1E). The cytokine production potential of each subset was assessed as an index of their suppressor and/or effector functions. We found higher IL-10 production potential in RORγt$^+$ T_{regs} and reduced IL-17A production potential in T_H17s from the DDX5$^{\Delta T}$ ileal lamina propria, suggesting that DDX5 regulates homeostatic CD4$^+$ T cell cytokine production capacities in the small intestine. DDX5 expression in colonic T cells is lower than those found in the ileum (Fig. 1D). IL-10 and IL-17A production potentials in colonic RORγt$^+$ T_{regs} and T_H17s were similar between CTL and DDX5$^{\Delta T}$ mice (Fig. 1F), suggesting that DDX5 did not modulate these homeostatic CD4$^+$ T cell cytokine production capacities in the colon.

DDX5 in T cells promotes intestinal inflammation

When challenged with the model of anti-CD3ε–induced enteropathy as previously described in (*26*, *27*), ileal and colonic T cells in CTL mice up-regulated DDX5 expression (Fig. 2A). To assess the contribution of DDX5 to the intestinal CD4$^+$ T population and their functions in an inflammatory setting, anti-CD3ε antibodies were administered to CTL and DDX5$^{\Delta T}$ cohoused littermates. For the first 48 hours, both groups experienced similar weight loss. By days 3 to 5, DDX5$^{\Delta T}$ mice gradually returned to normal weight, and their small intestine tissues showed milder pathology, while their cohoused CTL littermates maintained a 15 to 20% weight loss and sustained extensive epithelial tissue damage (Fig. 2B and fig. S2, A and B). These results indicate that DDX5 in T cells promotes intestinal inflammation.

In the inflamed DDX5$^{\Delta T}$ ileum, there was a significant reduction in the proportion and the absolute number of infiltrated CD4$^+$ T cells (fig. S3, A and B). Previous studies suggest that DDX5 can regulate immune cell survival and apoptosis in T cell acute lymphoblastic leukemia and acute myeloid leukemia (*17*, *28*). However, local proliferation and apoptosis of ileal T cells, as assessed by staining of Ki67 and annexin-V, were not influenced by the presence or absence of DDX5 (fig. S3C), suggesting that the reduced number of ileal CD4$^+$ T cells in the DDX5-deficient mice was not due to changes in local T cell proliferation and/or apoptosis. In the anti-CD3ε–challenged DDX5$^{\Delta T}$ ileum lamina propria, we found a higher proportion of cT_{regs}, IL-10$^+$ RORγt$^+$ T_{regs}, and a lower proportion of IL-17A$^+$ T_H17s (Fig. 2, C and D). IL-10 and IL-17A production potentials in ileal non-CD4 T cells were comparable in CTL and DDX5$^{\Delta T}$ mice (fig. S3D).

In the anti-CD3ε–challenged colon, the proportion and the absolute number of infiltrated CD4$^+$ T cells were modestly reduced in the absence of DDX5 (fig. S3, E and F) despite a reduction in the proportion of apoptotic cells (fig. S3G). Here, DDX5$^{\Delta T}$ RORγt$^+$ T_{regs} had elevated the IL-10 production capacity than controls (Fig. 2E), different from the observation made in the steady-state colon (Fig. 1F). The proportion of colonic IL-17A$^+$ T_H17 cells were similar between CTL and DDX5$^{\Delta T}$ mice (Fig. 2E). IL-10 and IL-17A production potentials in colonic non-CD4 cells were also comparable (fig. S3H). These results suggest that DDX5 regulates intestinal CD4$^+$ T cell population heterogeneity and cytokine production capacities in a context-dependent manner. The increase in ileal and colonic IL-10$^+$ RORγt$^+$ T_{regs} and/or reduction in ileal IL-17A$^+$ T_H17 cells may contribute to protecting the DDX5$^{\Delta T}$ mice from anti-CD3ε–induced enteropathy.

DDX5 negatively regulates RORγt$^+$ T_{reg} suppressor function in vitro and in vivo

Compared to cT_{regs}, RORγt$^+$ T_{regs} have elevated the expression of Cytotoxic T-Lymphocyte Associated Protein 4 (CTLA4) and C-C Motif Chemokine Receptor 6 (CCR6) (*10*, *11*). To test the role of DDX5 on RORγt$^+$ T_{reg} suppressor activity, we fluorescence-activated cell sorting (FACS)–sorted two T_{reg} populations, CCR6$^+$CTLA4$^+$ (enriched with 45 to 50% RORγt$^+$ T_{reg}) and CCR6$^-$ CD25$^+$ (enriched with 65 to 75% cT_{regs}) from the spleen and lymph nodes of CTL or DDX5$^{\Delta T}$ mice for the in vitro suppressor assay (Fig. 3A). Enriched DDX5$^{\Delta T}$ RORγt$^+$ T_{regs} showed significantly higher suppressor activity in 1:1 and 1:2 T_{reg}:T effector cell ratios than cells from CTL mice (Fig. 3B). In contrast, CTL and DDX5$^{\Delta T}$ cT_{reg}-enriched cells showed similar suppressor activity in most conditions except for DDX5$^{\Delta T}$ cT_{reg} showing reduced suppressor activity under the 1:1 condition. These results suggest that DDX5 can serve distinct functions in different T_{reg} subsets.

Next, we assessed the contribution of DDX5 to RORγt$^+$ T_{reg} suppressor activity in the T cell transfer colitis model. CTL or DDX5$^{\Delta T}$ CCR6$^+$CTLA4$^+$ T_{regs} were mixed with wild-type naïve effector T cells marked by CD90.1 in a 1:4 ratio and transferred to Recombination activating gene 1 knockout (Rag1$^{-/-}$) recipients. Between days 8 and 20, CTL and DDX5$^{\Delta T}$ T_{regs} showed comparable abilities in preventing weight loss in RAG1$^{-/-}$ recipients. By days 24 to 36, however, recipients of DDX5$^{\Delta T}$ CCR6$^+$CTLA4$^+$ T_{regs} experienced less weight loss compared to those receiving CTL CCR6$^+$CTLA4$^+$ T_{regs} (Fig. 3C). Recipients of DDX5$^{\Delta T}$ CCR6$^+$CTLA4$^+$ T_{regs} had a slight, although not significant, reduction of total mononuclear cells and effector T cells in the colonic lamina propria (Fig. 3D) and slight reductions in *Il17a* and *Il23a* transcript abundance (Fig. 3E). DDX5$^{\Delta T}$ CCR6$^+$CTLA4$^+$ cells maintained a higher proportion of IL-10 producers in the colonic lamina propria and spleen (Fig. 3F). In contrast, IL-10 production potential in cells derived from the wild-type naïve effector T cells marked by CD90.1 was not influenced by DDX5 levels in neighboring cells (Fig. 3F), suggesting that DDX5 likely modulate IL-10 production capacity in CCR6$^+$CTLA4$^+$ cells in a cell-intrinsic manner. Together, these results demonstrate that DDX5 negatively regulates RORγt$^+$ T_{reg} suppressor function in vitro and in vivo.

Inhibition of IL-10 signaling restores enteropathy susceptibility in DDX5-deficient mice

To test the extent IL-10 signaling contributes to the differential weight changes observed in the anti-CD3ε–challenged mice, CTL and DDX5$^{\Delta T}$ mice were treated with anti–IL-10R blocking antibodies or isotype controls. Notably, anti-IL-10R–treated DDX5$^{\Delta T}$ mice were no longer protected from anti-CD3ε–induced weight loss on days 4 to 5 (Fig. 4A). These results suggest that the protective effect from DDX5-deficient T cells is dependent on IL-10 signaling, presumably in both T and non–T cells.

To determine whether DDX5 regulated IL-10 expression in T cells through a cell-intrinsic or paracrine mechanism, CD90.1-marked CTL and tdTomato-marked DDX5$^{\Delta T}$ T cells were cotransferred in a 1:1 ratio into CTL recipients. Following anti-CD3ε administration, tdTomato-marked DDX5$^{\Delta T}$ RORγt$^+$ T_{regs} harbored higher IL-10 production potential than the CD90.1-marked CTL RORγt$^+$ T_{regs} (Fig. 4B), indicating that DDX5 restricted IL-10 production in RORγt$^+$ T_{regs} through a cell-intrinsic mechanism.

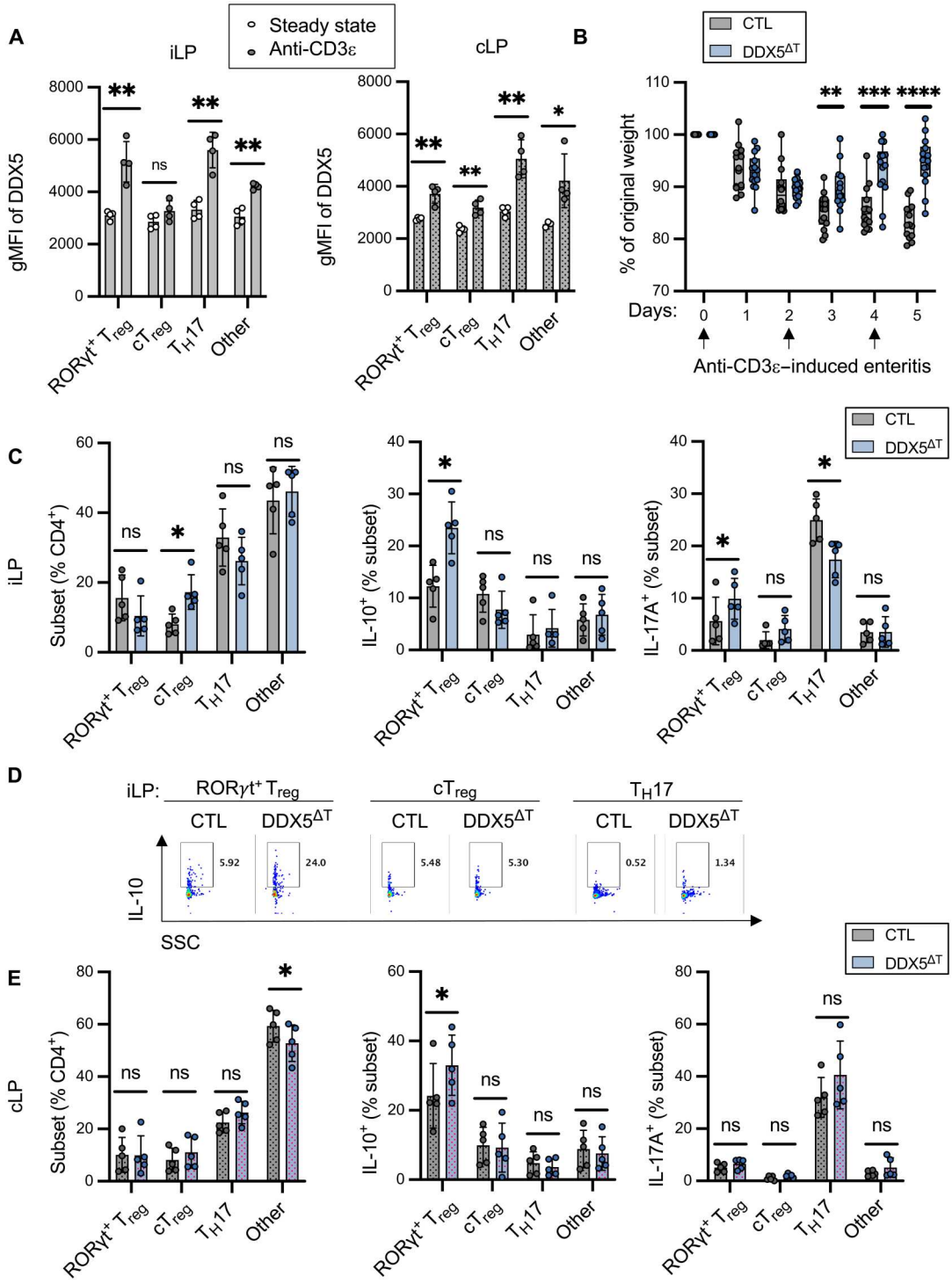

Fig. 2. DDX5 in T cells promotes intestinal inflammation. (**A**) gMFI of DDX5 in the indicated T cell subsets from iLP and cLP of steady-state or anti-CD3ε–challenged wild-type mice. Each dot represents the result from one mouse. *$P < 0.05$ and **$P < 0.01$ (paired multiple *t* test, $n = 4$). (**B**) Weight changes of CTL and DDX5$^{\Delta T}$ gender-matched cohoused littermates intraperitoneally challenged with anti-CD3ε monoclonal antibodies (mAb) on days 0, 2, and 4 as indicated. **$P < 0.01$, ***$P < 0.001$, and ****$P < 0.0001$ (paired multiple *t* test, $n = 14$, combined from three independent experiments). (**C**) Proportions of the indicated subsets among CD4$^+$ T cells and their IL-10 and IL-17A production potential in iLP from inflamed CTL and DDX5$^{\Delta T}$ littermates. *$P < 0.05$ (paired multiple *t* test, $n = 5$). (**D**) Representative flow cytometry analysis of IL-10 in ileal CD4$^+$ T cell subsets from CTL and DDX5$^{\Delta T}$ mice administrated with anti-CD3ε. SSC, side scatter as an index of cell granularity. (**E**) Proportions of the indicated subsets among CD4$^+$ T cells and their IL-10 and IL-17A production potential in cLP from inflamed CTL and DDX5$^{\Delta T}$ littermates. *$P < 0.05$ (paired multiple *t* test, $n = 5$).

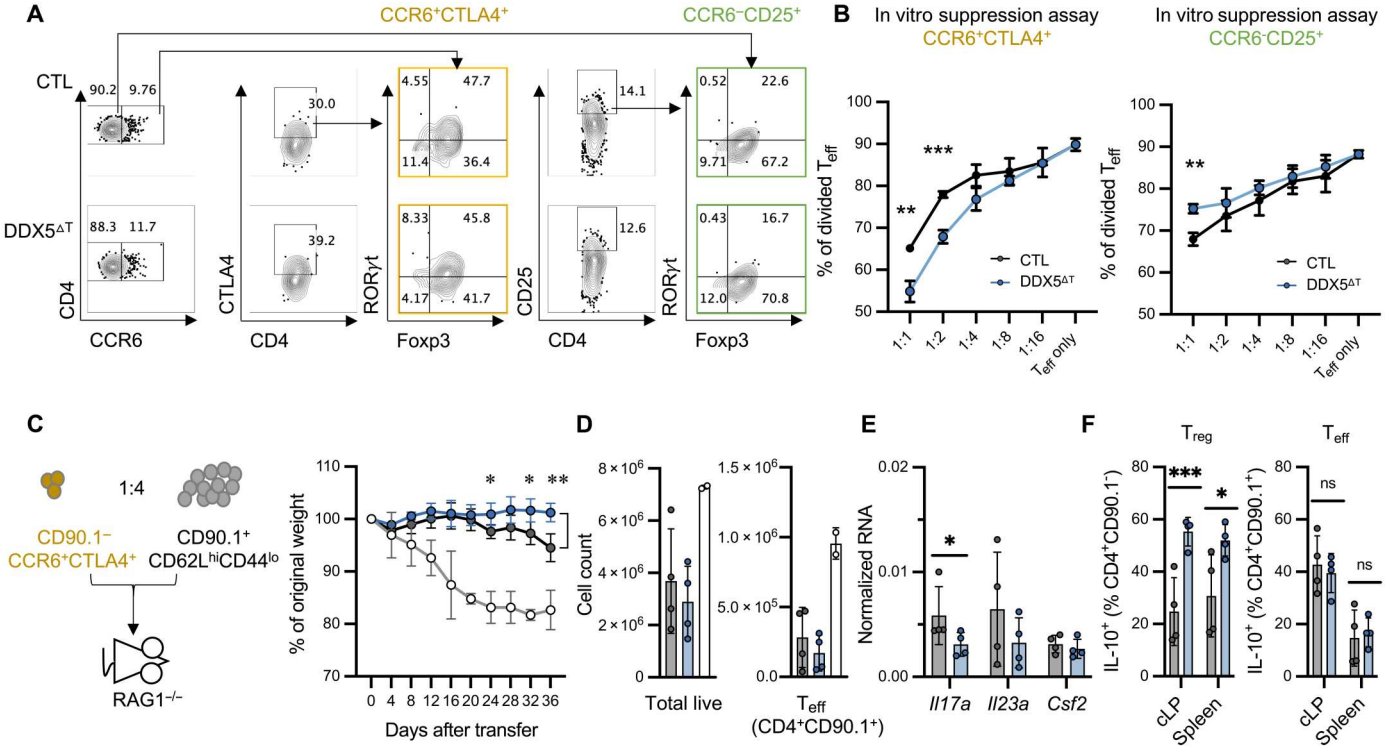

Fig. 3. DDX5 negatively regulates RORγt$^+$ T_{reg} suppressor function in vitro and in vivo. (**A**) Gating strategy for FACS sorting the CCR6$^-$CD25$^+$ (enriched with 65 to 75% cT_{regs}) and CCR6$^+$CTLA4$^+$ (enriched with 45 to 50% RORγt$^+$ T_{regs}) populations. (**B**) Proliferation index of wild-type naïve cells (CD4$^+$CDD62L^{hi}CD44^{lo}) cocultured with CCR6$^-$CD25$^+$ and CCR6$^+$CTLA4$^+$ cells from CTL or DDX5$^{\Delta T}$ mice in the indicated ratio for 72 hours. Average and SD from three replicates are shown. $^{**}P < 0.01$ and $^{***}P < 0.005$ (multiple *t* tests). (**C**) Left: Experiment scheme. Right: Weight changes of RAG1$^{-/-}$ recipients of wild-type naïve CD4$^+$ T cells (white circles, $n = 2$), naïve cells together with CTL CCR6$^+$CTLA4$^+$ (black circles, $n = 4$), or naïve cells together with DDX5$^{\Delta T}$ CCR6$^+$CTLA4$^+$ cells (blue circles, $n = 4$). $^*P < 0.05$ and $^{**}P < 0.01$ (multiple *t* tests). (**D**) Total cLP mononuclear cell counts and CD4$^+$ T effector (T_{eff}) cell counts derived from the wild-type naïve donor on day 36 after T cell transfer in mice described in (C). (**E**) Normalized mRNA expression of the indicated cytokine genes in cLP mononuclear cell lysates from mice described in (C). $^*P < 0.05$ (multiple *t* tests). (**F**) Proportions of IL-10 production potential in transferred T_{reg} (CD90.1$^-$) and T effector (CD90.1$^+$) populations on day 36 after T cell transfer in mice described in (C). Each dot represents the result from one mouse. $^*P < 0.05$ and $^{***}P < 0.005$ (multiple *t* tests).

DDX5 RNA interactome in cultured T cells

Next, we used a culture system as previously described (*29*, *30*) where purified naïve CD4$^+$ T cells were polarized toward RORγt$^+$ T_{reg}-like cells in the presence of IL-6 (20 ng/ml) and elevated concentration of transforming growth factor–β (TGFβ; 5 ng/ml) to identify the direct RNA targets of DDX5 (fig. S4, A and B). DDX5$^{\Delta T}$ cells generated in this condition also displayed augmented IL-10 production capacities (Fig. 4C), similar to our in vivo observation (Figs. 1E and 2, C to E). To identify DDX5-bound RNAs, cultured CTL cells were ultraviolet (UV)–cross-linked for the enhanced cross-linked immunoprecipitation sequencing (eCLIP-seq) assay (fig. S5A). Global analysis revealed that DDX5 binding to intronic regions near coding sequences (proximal intron) accounts for the largest fraction of its RNA interactome in T cells (Fig. 4D), similar to findings reported in other cell types (*25*, *31*). However, we did not detect any DDX5 signals on *Il10* transcripts, suggesting that DDX5 likely regulated IL-10 expression through a more elaborate mechanism.

DDX5 controls RORγt$^+$ T_{reg} function and promotes enteropathy by repressing HIF1α

Among the transcripts encoding molecules previously implicated in regulating IL-10 levels in other cell types, *Hif1a* was bound by DDX5 (Fig. 4E). In cancer cells, DDX5 has been reported to potentiate *Hif1a* expression (*32*). In contrast, knocking out DDX5 in culture RORγt$^+$ T_{reg}-like cells resulted in a significant elevation of *Hif1a* at both the RNA and protein levels (Fig. 4, F and G). In T_H1 cells, hypoxia and HIF1α are positive regulators of IL-10 (*33*); therefore, we hypothesized that DDX5 regulation of *Hif1a* in RORγt$^+$ T_{reg}-like cells might similarly affect their IL-10 production potential. DDX5$^{\Delta T}$ RORγt$^+$ T_{reg}-like cells displayed a significant increase of the HIF1α$^+$IL-10$^+$ population (Fig. 4H).

In the ileal lamina propria under steady state, RORγt$^+$ T_{regs} and cT_{regs} had the highest HIF1α expression (Fig. 5A). Ablation of DDX5 resulted in elevated HIF1α protein levels in RORγt$^+$ T_{regs} and not in any other CD4 T cell subsets (Fig. 5A), suggesting that DDX5 regulated HIF1α in a cell type–specific manner. On the basis of these results, we hypothesized that IL-10 production in RORγt$^+$ T_{regs} might be regulated by the DDX5-HIF1α axis and that DDX5 regulation of IL-17A production in ileal T_H17 cells (Fig. 1E) was through a HIF1α-independent mechanism. We detected a higher proportion of HIF1α$^+$IL-10$^+$ RORγt$^+$ T_{regs} in the steady-state and inflamed DDX5$^{\Delta T}$ ileum (Fig. 5, B and C), as well as in the inflamed DDX5$^{\Delta T}$ colon after anti-CD3ε administration (fig. S6, A and B). These results demonstrate that DDX5 regulates IL-10 and HIF1α expressions in intestinal RORγt$^+$ T_{regs}.

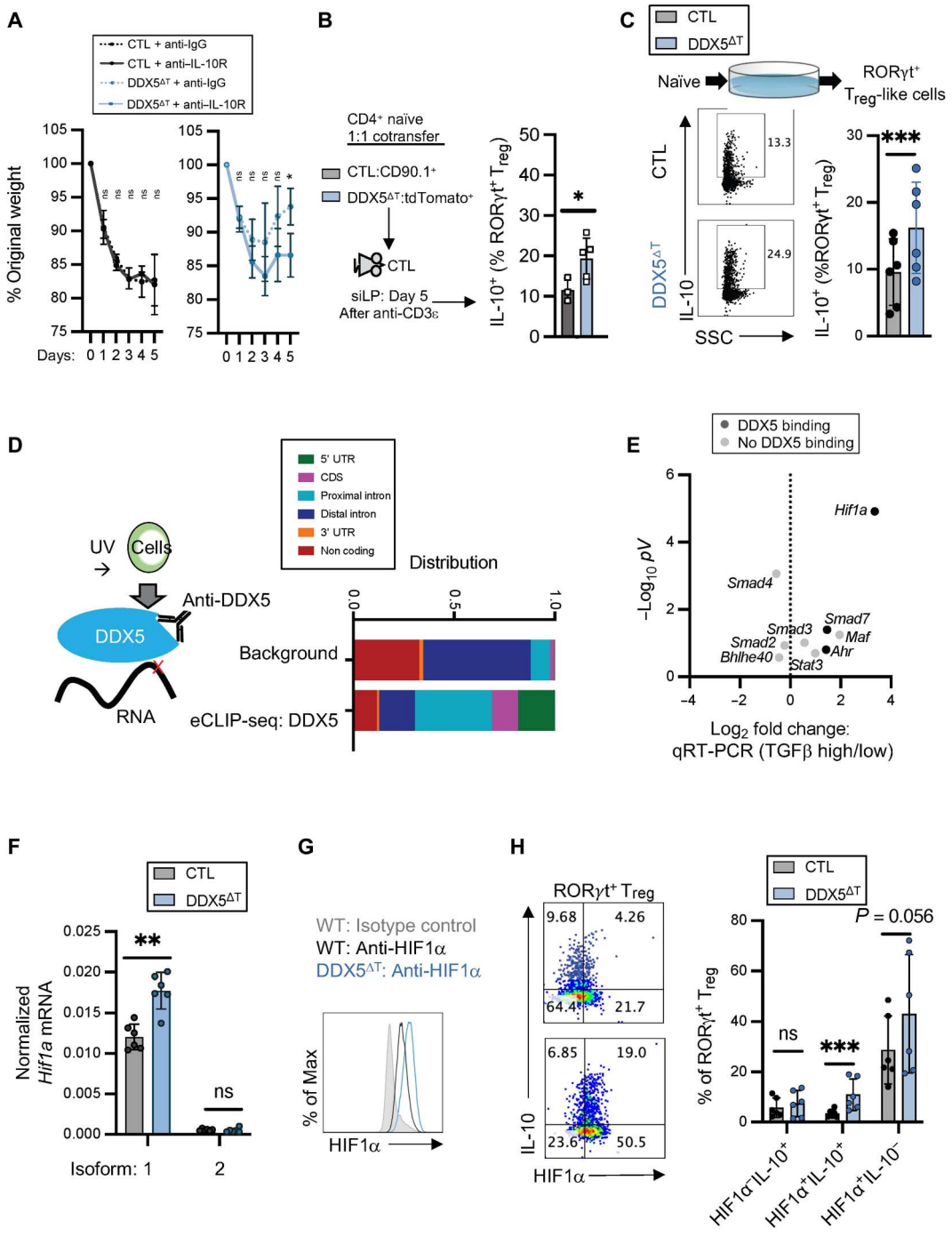

Fig. 4. Identifying DDX5 targets in T cells. (**A**) Weight changes of cohoused CTL and DDX5$^{\Delta T}$ littermates administered with anti-CD3ε and anti-rat IgG (isotype control) or anti–IL-10R intraperitoneally on days 0, 2, and 4. *$P < 0.05$ (paired multiple *t* tests, $n = 4$). (**B**) CD90.1$^+$ CTL or tdTomato$^+$ DDX5$^{\Delta T}$ naïve CD4$^+$ T cells cotransfer into wild-type mice. iLP T cell cytokine levels were analyzed 5 days after anti-CD3ε challenge. *$P < 0.05$ (*t* test). (**C**) IL-10 levels in cultured RORγt$^+$ T_{reg}-like cells ($n = 6$). (**D**) Distribution of DDX5-bound RNA regions in cultured T cells. 5′-UTR, 5′ untranslated region. (**E**) Expression of select mRNAs. Log_2 fold changes were defined by qRT-PCR results normalized to *Gapdh* from T cells cultured in the TGFβ (5 ng/ml, high) over those under the TGFβ (0.1 ng/ml, low) condition (multiple *t* tests, $n = 4$). Black dot: Enriched with DDX5 eCLIP-seq signal; gray dot: DDX5 eCLIP-seq signal absent. (**F**) Normalized mRNA levels of two *Hif1a* isoforms in cultured RORγt$^+$ T_{reg}-like cells. Each dot represents the result from one mouse. **$P < 0.01$ (paired multiple *t* test, $n = 6$). (**G**) Representative histogram of isotype or HIF1α in cultured RORγt$^+$ T_{reg}-like cells. (**H**) Representative flow plots (left) and proportions (right, each dot represents the result from one mouse) of HIF1α and IL-10 expression in cultured RORγt$^+$ T_{reg}-like cells. ***$P < 0.001$ (paired multiple *t* test, $n = 6$).

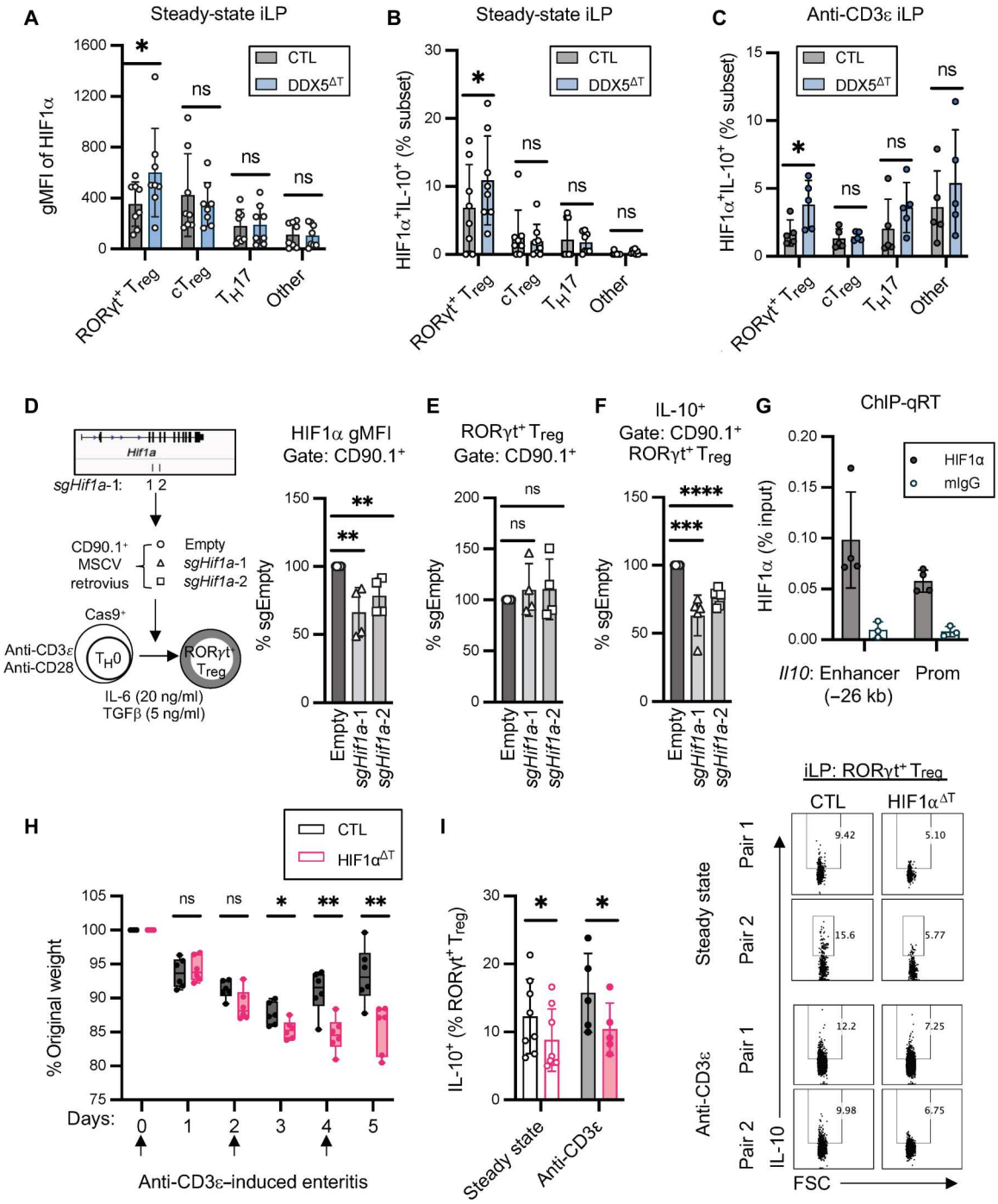

Fig. 5. HIF1α regulates RORγt$^+$ T$_{reg}$ suppressor function. (**A**) gMFI of HIF1α in the indicated iLP subsets from steady-state CTL and DDX5$^{\Delta}$ mice. Each dot represents the result from one mouse. *P < 0.05 (paired multiple t test, n = 8). (**B**) HIF1α$^+$IL-10$^+$ proportions among the indicated iLP subsets from steady-state mice. Each dot represents the result from one mouse. *P < 0.05 (paired multiple t test, n = 8). (**C**) HIF1α$^+$IL-10$^+$ proportions among the indicated iLP subsets from anti-CD3ε–challenged mice. Each dot represents the result from one mouse. *P < 0.05 (paired multiple t tests, n = 5). (**D**) Left: Workflow for Cas9-sgRNA–mediated knockdown of HIF1α. Right: gMFI of HIF1α in transduced cultured Cas9$^+$ T cells normalized to results from sgEmpty. MSCV, Murine Stem Cell Virus. Each dot represents the result from one mouse. **P < 0.01 (t test, n = 4). (**E**) RORγt$^+$ T$_{reg}$-like cells proportions among transduced cells from (D) normalized to results from sgEmpty. ns, not significant (t test, n = 4). (**F**) IL-10$^+$ proportion among the transduced RORγt$^+$ T$_{reg}$-like cells normalized to results from sgEmpty. Each dot represents the result from one mouse. ***P < 0.005 and ****P < 0.001 (t test, n = 4). (**G**) HIF1α occupancy on the *Il10* locus in cultured RORγt$^+$ T$_{reg}$-like cells. mIgG, mouse immunoglobulin G. Each dot represents the result from one mouse. **P < 0.01 (paired multiple t tests, n = 4). (**H**) Weight changes of indicated mice after anti-CD3ε mAb challenge. **P < 0.01 (paired multiple t tests, n = 6). (**I**) Proportion of IL-10–expressing RORγt$^+$ T$_{regs}$ from steady-state or anti-CD3ε–challenged mice. FSC, forward scatter as an index of cell granularity. *P < 0.05 (paired multiple t test).

To test the contribution of HIF1α to IL-10 production in RORγt$^+$ T$_{regs}$, we knocked down HIF1α using two independent single guide RNAs (sgRNAs) designed to target either exon 3 (sg*Hif1a*-1) or exon 4 (sg*Hif1a*-2) at the *Hif1a* locus in cultured RORγt$^+$ T$_{reg}$-like cells derived from CTL Cas9$^+$ mice (Fig. 5D). While the transient loss of HIF1α did not alter RORγt expression (Fig. 5E), it resulted in a significant reduction of IL-10 production capacity in the RORγt$^+$ T$_{reg}$-like cells (Fig. 5F). Chromatin immunoprecipitation quantitative polymerase chain reaction (ChIP-qPCR) assays revealed that HIF1α was recruited to the *Il10* promoter and a distal enhancer 26-kb upstream of the transcription start site (Fig. 5G), indicating that HIF1α could directly regulate the *Il10* locus in RORγt$^+$ T$_{reg}$-like cells. Consistent with this possibility, inhibition of HIF1α DNA binding by echinomycin effectively reduced IL-10 production potential in cultured DDX5$^{\Delta T}$ RORγt$^+$ T$_{regs}$-like cells to levels observed in CTL cells in a dose-dependent manner (fig. S7, A and B). A previous study in cT$_{regs}$ reported that HIF1α controls the expression of genes involved in glycolysis (*6*). In RORγt$^+$ T$_{reg}$-like cells, however, we did not observe a similar dependency of glycolysis genes on DDX5 (fig. S7C).

When challenged with anti-CD3ε, HIF1α$^{\Delta T}$ (*Hif1a$^{fl/fl}$Cd4^{Cre}*) mice showed more weight loss (Fig. 5H) and higher ileal pathology compared to their CTL littermates (fig. S8, A and B). Under both basal and inflamed settings in vivo, ileal HIF1α$^{\Delta T}$ RORγt$^+$ T$_{reg}$ cells showed lowered IL-10 production potential (Fig. 5I), demonstrating that HIF1α promotes IL-10 expression in RORγt$^+$ T$_{regs}$ in vivo. To test the hypothesis that the enteropathy protection found in DDX5$^{\Delta T}$ mice was conferred by the augmented expression of HIF1α in their T cells, we crossed the DDX5$^{\Delta T}$ mice with the HIF1α$^{\Delta T}$ line to generate the DDX5$^{\Delta T}$HIF1α$^{\Delta T}$ double knockout mice (*Hif1a$^{fl/fl}$ Ddx5$^{fl/fl}$ Cd4^{Cre}*). When challenged with anti-CD3ε, DDX5$^{\Delta T}$HIF1α$^{\Delta T}$ mice experienced similar weight loss compared to CTL mice (Fig. 6A). The ileal CD4$^+$ infiltrate proportion and absolute number in the DDX5$^{\Delta T}$HIF1α$^{\Delta T}$ mice were partially restored to CTL levels (Fig. 6B). Notably, DDX5$^{\Delta T}$HIF1α$^{\Delta T}$ RORγt$^+$ T$_{regs}$ harbored similar levels of IL-10 as CTL (Fig. 6, C and D). Similarly, the pharmacologic inhibition of HIF1α DNA binding also obliterated the differences in weight, intestine pathology, total T cell count, and IL-10$^+$ RORγt$^+$ T$_{reg}$ populations between CTL and DDX5$^{\Delta T}$ littermates (Fig. 6, E to H). Together, these results show that DDX5 promotes enteropathy and restricts IL-10 production in RORγt$^+$ T$_{reg}$ in a HIF1α-dependent manner (modeled in Fig. 6I).

DDX5 promotes R loop disassembly and restricts RNA Pol2 recruitment on the *Hif1a* locus in RORγt$^+$ T$_{regs}$

To evaluate the contribution of DDX5 binding on the *Hif1a* transcripts toward its repressive activity on *Hif1a* expression, we designed a sgRNA (sg*Hif1a*^{DB}) targeting the intron encoding the DDX5 binding sites (Fig. 7A). As expected, cultured Cas9$^+$ RORγt$^+$ T$_{reg}$-like cells transduced with the sg*Hif1a*^{DB} expressing vector had a higher proportion of HIF1α$^+$IL-10$^+$ cells (Fig. 7B). These results suggest that the DDX5 bound stretch of intron 1 on the *Hif1a* transcript confers repressive activities on HIF1α and IL-10 expressions in cultured RORγt$^+$ T$_{reg}$-like cells.

A recent study report that the *HIF1A* locus in human epithelial cells is enriched with DNA-RNA hybrid (R loop) structures (*34*) implicated in transcription regulation (*35*–*37*). In addition, DDX5-mediated R loop resolution can promote RNA polymerase II (Pol2) transcription termination (*18*, *19*, *23*, *24*). To test whether DDX5 also regulated the murine *Hif1a* locus through an R loop–dependent mechanism, we performed the DNA-RNA immunoprecipitation (DRIP) assay using the S9.6 antibodies on cultured RORγt$^+$ T$_{reg}$-like cells. Similar to human cells, the murine *Hif1a* locus was also decorated with R loop structures at the transcriptional start and terminal sites (Fig. 7C). Loss of DDX5 resulted in an accumulation of R loop signals that paralleled an increase in the occupancy of RNA Pol2 and H3K4me3 deposition at the *Hif1a* transcription start site (Fig. 7D). After transcription, the splicing rate of the *Hif1a* nascent transcripts and the RNA half-life of the mature *Hif1a* mRNA were comparable between CTL and DDX5$^{\Delta T}$ cells (fig. S9, A to C), suggesting that DDX5 regulated *Hif1a* at the transcription level. Together, these results demonstrate that DDX5 regulates R loop structures and RNA Pol2 recruitment to restrict *Hif1a* transcription in RORγt$^+$ T$_{regs}$ (modeled in Fig. 7E).

RX-5902 is a small-molecule inhibitor developed to target DDX5 (*38*). As expected, the proportion of HIF1α$^+$IL-10$^+$ RORγt$^+$ T$_{reg}$-like cells was elevated in the presence of RX-5902 (Fig. 7F), consistent with results observed using genetic approaches. Similarly, human Jurkat T cells cultured in the presence of RX-5902 also had a higher proportion of HIF1α$^+$IL-10$^+$ cells (Fig. 7, G and H). Furthermore, analysis of two publicly available datasets of human ileal T cells also suggests that *HIF1A* mRNA abundance positively correlates with *IL10* transcript levels (Fig. 7I). Together, these results suggest that pharmacologic inhibition of DDX5 can modulate the HIF1α–IL-10 pathway in both mouse and human T cells.

DISCUSSION

Anti-inflammatory cytokine IL-10 is critical for maintaining tissue homeostasis and preventing exacerbated inflammation after injury (*39*–*42*). Previous studies identified multiple T cell subsets with IL-10 production capacities under different settings, including T$_H$17 (*43*), T$_H$1 (*33*), cT$_{regs}$ (*44*), RORγt$^+$ T$_{regs}$ (*10*), and CD8$^+$ T cells (*45*). Here, we show that ileal and colonic RORγt$^+$ T$_{regs}$ have the highest IL-10 production potential among T cells, and this is transcriptionally controlled by HIF1α. In the steady-state and inflamed small intestine, the HIF1α–IL-10 pathway in RORγt$^+$ T$_{regs}$ is inhibited by the RNA binding protein DDX5. In the steady-state colon, however, DDX5 does not regulate IL-10 or IL-17A production in RORγt$^+$ T$_{regs}$ or T$_H$17 cells. DDX5-dependent RORγt$^+$ T$_{regs}$ only emerge in the colonic lamina propria after anti-CD3ε challenge. The exact origin of these DDX5-dependent colonic RORγt$^+$ T$_{regs}$ is not known. One possibility is that these cells are RORγt$^+$ T$_{regs}$ from the ileum that migrated to the colon after anti-CD3ε challenge. Another possibility may be that these are local RORγt$^+$ T$_{regs}$ that acquired a DDX5-dependent program in the inflammatory environment. Unlike T cells, DDX5 in cancer cells can serve as a positive regulator of HIF1α (*32*). These results suggest that the positive or negative regulation of HIF1α by DDX5 is cell type and context dependent, and future studies are needed to identify the molecular determinants involved in orchestrating these specificities.

In RORγt$^+$ T$_{regs}$, knocking out DDX5 results in an increase of HIF1α and IL-10 levels, as well as greater contact-dependent suppressor activities in vitro and in vivo. When challenged with the anti-CD3ε–induced and T cell transfer–mediated intestinal inflammation, DDX5$^{\Delta T}$ RORγt$^+$ T$_{regs}$ provide superior protection against weight loss and tissue pathology. Pharmacologic inhibition of IL-10

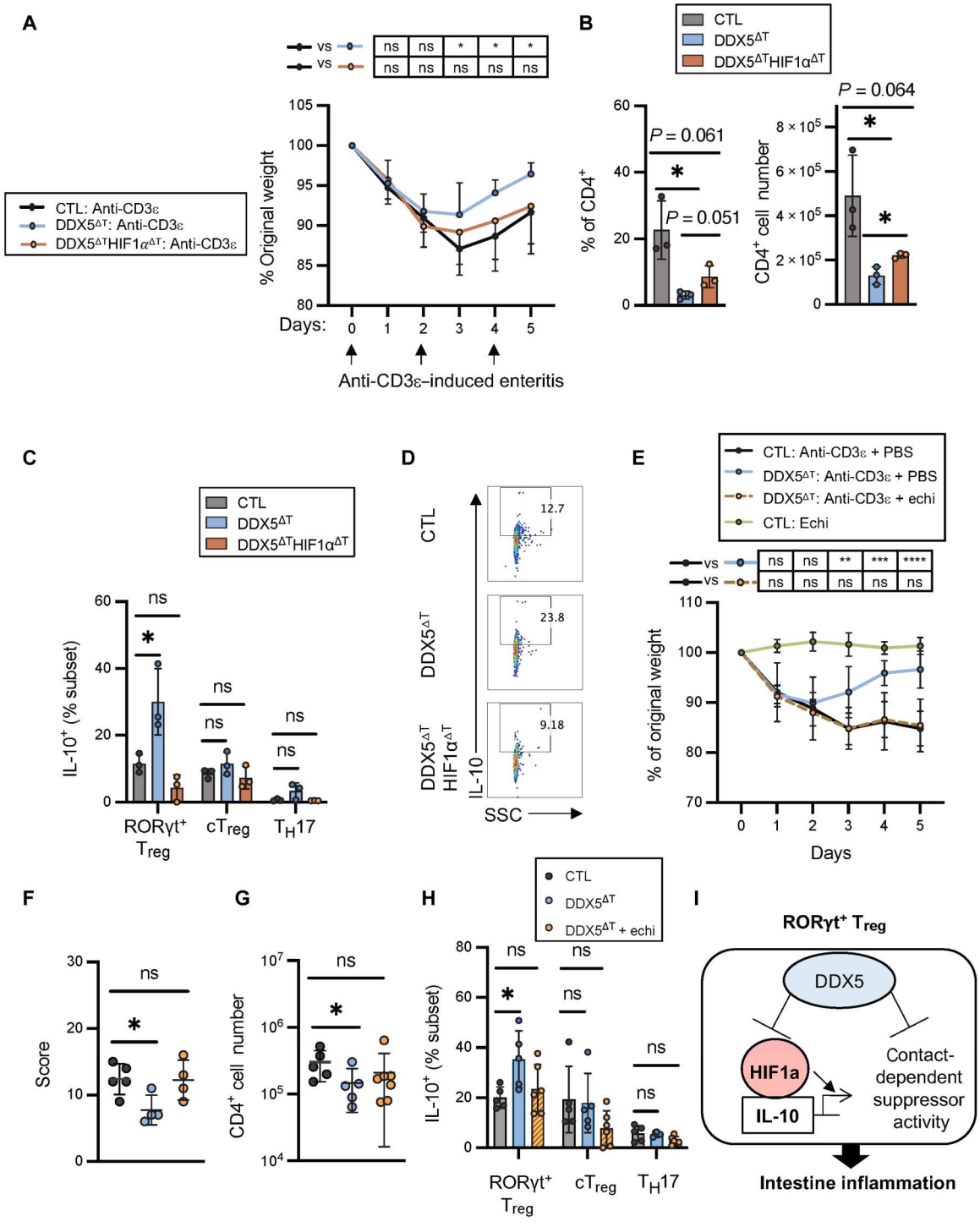

Fig. 6. Genetic ablation of HIF1α or inhibition of HIF1α DNA binding restores enteropathy susceptibility in DDX5$^{\Delta T}$ mice. (**A**) Weight changes of three pairs of CTL, DDX5$^{\Delta T}$, and DDX5$^{\Delta}$HIF1α$^{\Delta T}$ mice administered with anti-CD3ε mAb. *P < 0.05 (multiple t tests, n = 3). (**B**) Proportions (left) and number (right) of ileal CD4$^+$ T cell in the mice as shown in (A). *P < 0.05 (t test, n = 3). (**C**) Proportions of IL-10$^+$ ileal CD4$^+$ T cell subsets from (B). Each dot represents the result from one mouse. *P < 0.05 (t test). (**D**) Representative flow cytometry analysis of IL-10 in ileal CD4$^+$ T cell subsets from indicated mice administrated with anti-CD3ε. (**E**) Weight changes of five pairs of CTL and DDX5$^{\Delta T}$ mice administered with anti-CD3ε mAb or anti-CD3ε mAb and echinomycin (100 μg/kg) or echinomycin alone (100 μg/kg). **P < 0.01, ***P < 0.005, and ****P < 0.001 (multiple t tests). (**F**) Disease score of ileal sections from (E). (**G**) Ileal CD4$^+$ T cell count from (E). Each dot represents the result from one mouse. *P < 0.05 (t test). (**H**) Proportions of IL-10$^+$ ileal CD4$^+$ T cell subsets from (E). Each dot represents results from one mouse. *P < 0.05 (t test). (**I**) Working model: DDX5 inhibits HIF1α-mediated IL-10 expression and contact-dependent suppressor function in RORγt$^+$ T_{reg} and promotes T cell–mediated inflammation in the intestine.

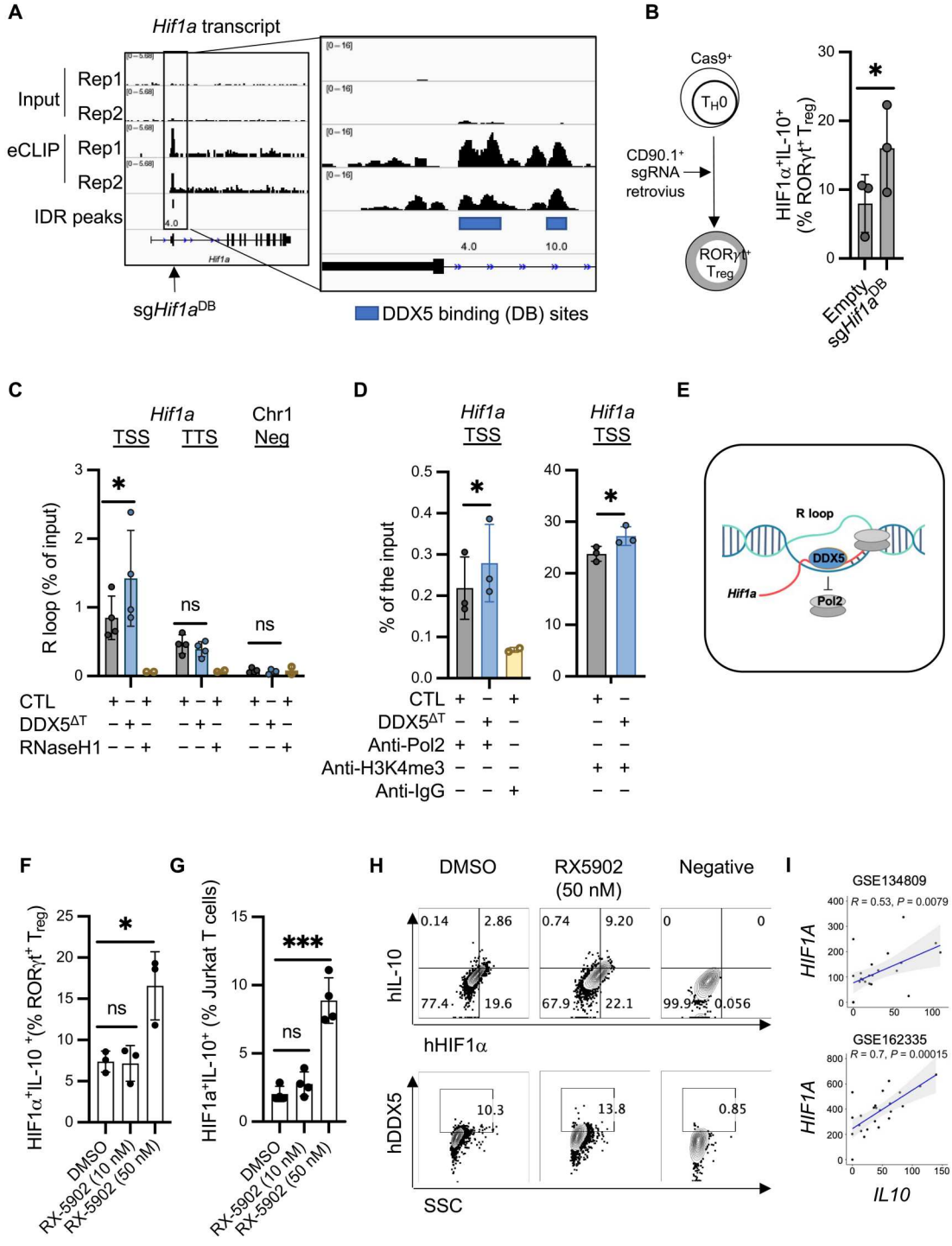

Fig. 7. DDX5 promotes R loop disassembly and restricts RNA Pol2 recruitment to repress *Hif1a* transcription. (**A**) DDX5-bound regions on the *Hif1a* transcript. (**B**) HIF1α$^+$IL-10$^+$ proportions in cultured Cas9$^+$ RORγt$^+$ T$_{reg}$-like cells transduced with the indicated retroviruses. Each dot represents the result from one mouse. *P < 0.05 (t test). (**C**) DRIP-qRT detection of RNA-DNA hybrid structures in cultured RORγt$^+$ T$_{reg}$-like cells. TSS, Transcription Start Site; TTS, Transcription Termination Site. Each dot represents the result from one mouse. *P < 0.05 (paired multiple t tests, n = 4). RNaseH1, ribonuclease H1. (**D**) RNA Pol2 and H3K4me3 ChIP-qPCR analysis at the *Hif1a locus* in cultured RORγt$^+$ T$_{reg}$-like cells. Each dot represents the result from one mouse. *P < 0.05 (paired multiple t test, n = 3). (**E**) Working model: DDX5 resolves the R loop to block RNA Pol2 loading and inhibit *Hif1a* transcription. (**F**) HIF1α$^+$IL-10$^+$ proportions in cultured RORγt$^+$ T$_{reg}$-like cells treated with vehicle [dimethyl sulfoxide (DMSO)] or the DDX5 inhibitor (RX-5902) for 72 hours. Each dot represents the result from an independent experiment. *P < 0.05 (t test). (**G**) HIF1α$^+$IL-10$^+$ proportions in human Jurkat T cells treated with vehicle (DMSO) or the DDX5 inhibitor (RX-5902) for 72 hours. Each dot represents the result of an independent experiment. ***P < 0.001 (t test, n = 4). (**H**) Representative staining of HIF1α, IL-10, DDX5, and isotype (negative) in human Jurkat T cells. h, human. (**I**) *HIF1A* and *IL10* expressions in human ileal RORγt$^+$ T$_{regs}$ as determined by single-cell RNA sequencing [GSE134809 (*53*) and GSE162335 (*54*)]. Each dot represents the average expression of these genes from one donor.

signaling restores the anti-CD3ε susceptibility of the DDX5$^{\Delta T}$ mice to wild-type levels, suggesting that DDX5 promotes inflammation, at least in part, by negatively regulating IL-10. Because DDX5 also positively regulates IL-17A in ileal T_H17 cells, we cannot rule out the possibility that this also contributes to the altered anti-CD3ε susceptibility in DDX5$^{\Delta T}$ mice. The in vitro suppressor assay also indicates that DDX5 can interfere with the contact-dependent suppressor activity of RORγt$^+$ T_{regs}. However, it remains to be explored the extent this regulation of DDX5 on RORγt$^+$ T_{regs} contributes to the protective phenotypes observed in vivo.

At the molecular level, DDX5 binding to the first intron of the *Hif1a* transcript promotes R loop resolution and restricts RNA Pol2 recruitment to the *Hif1a* promoter. This study provides the first in vivo and mechanistic evidence that an imbalance of R loop–associated RNA binding proteins can modulate immune cell function and contribute to intestinal pathologies. Future studies will be needed to assess the extent DDX5 contributes to chromatin R loop dynamics genome-wide and whether other members of this RNA binding protein family have unique or overlapping functions as DDX5. We speculate this negative feedback switch is evolutionarily conserved to keep T_{reg} suppressor activities in check and to allow for a robust inflammatory response in settings of infection and tissue injury.

In contrast to the proinflammatory role in T cells reported here, DDX5 in the intestinal epithelial cells is reported to be protective against the same model of T cell–mediated enteropathy (*12*). This highlights the importance of understanding how DDX5 regulates expressions of common and cell type–specific RNA targets to decipher its paradoxical contribution to intestinal pathologies and the therapeutic potential of these DDX5-dependent pathways for combating T cell–mediated inflammation in the intestine.

MATERIALS AND METHODS

Mice

Cas9 (stock no: 026179), *Cd4*^{Cre} (stock no: 017336), *Hif1a*^{flox} mice (stock no: 007561), and RAG1$^{-/-}$ (stock no: 002216) mice were obtained from the Jackson Laboratory. *Ddx5*^{flox} mice were obtained from F. Fuller-Pace's laboratory and have been previously described in (*46*). Heterozygous mice were bred to yield 6- to 12-week-old littermates. All animal studies were approved and followed the Institutional Animal Care and Use Guidelines of the University of California San Diego.

Anti-CD3ε–induced enteropathy model

Adult mice of 8 to 12 weeks were used for anti-CD3ε–induced enteropathy. Anti-CD3ε monoclonal antibodies (mAb) (15 μg per time per mouse; eBioscience, clone #: 2C11) with or without anti–IL-10R (0.2 mg per time per mouse; Bio X Cell, clone #: CD210) or anti-rat immunoglobulin G1 (IgG1) (Bio X Cell, BE0088) were injected intraperitoneally at days 0, 2, and 4. Ileal tissues were harvested on day 5. Ileal tissues were collected for hematoxylin and eosin (H&E) staining, and lamina propria cells were isolated for flow cytometry analysis as described in (*47*). The H&E slides from each sample were scored for changes in the inflammatory infiltrate, submucosal inflammation, crypt morphology, muscle thickening, and abscess in a double-blind fashion as described in (*25*).

For cotransfer experiments, splenic naïve CD4$^+$ T cells from CD90.1$^+$ CTL and tdTomato$^+$ DDX5$^{\Delta T}$ donors were isolated using the Naïve CD4$^+$ T Cell Isolation Kit (Miltenyi Biotec). CTL and DDX5$^{\Delta T}$ cells were combined in a 1:1 ratio (0.5 million each, a total of 1 million in phosphate-buffered saline) and transferred into CTL mice by intraperitoneal injection. After 1 week, recipient CTL mice were challenged with anti-CD3ε to induce enteropathy. Lamina propria cells were isolated for flow cytometry analysis. For transfer colitis, each RAG1$^{-/-}$ mouse was intraperitoneally injected with FACS-sorted CD90.1$^+$ naïve T helper cells (CD4$^+$CD25$^-$CD44^{lo}CD62L^{hi}, 0.4 million) and RORγt$^+$ T_{reg}-enriched cells (CD90.1$^-$CD4$^+$CCR6$^+$CTLA4$^+$, 0.1 million) from the spleen and lymph nodes.

In vitro suppressor assay

CCR6$^-$CD25$^+$ and CCR6$^+$CTLA4$^+$ cells from the spleen and lymph nodes of CD45.2$^+$ mice were FACS-sorted by MA900 (Sony) and mixed with FACS-sorted CD45.1$^+$ naïve CD4$^+$ T cells labeled with CellTrace Violet (Thermo Fisher Scientific, #C34571) in the presence of irradiated T cell–depleted splenocytes as antigen-presenting cells. After 3 days of coculture in RPMI 1640 containing 10% fetal bovine serum (FBS), T_{reg} suppression function was measured by the percentage of nondividing cells within the CD45.1$^+$ effector T cell population.

Flow cytometry

Ileal and colonic lamina propria mononuclear cells were obtained as previously described (*47*). Cells were stimulated with phorbol 12-myristate 13-acetate (5 ng/ml; MilliporeSigma) and ionomycin (500 ng/ml; MilliporeSigma) in the presence of GolgiStop (BD Biosciences) for 5 hours at 37°C, followed by cell surface marker staining for CD4 (clone GK1.5, BioLegend) and CD90.1/Thy1.1 (clone OX-7, BioLegend). Fixation/permeabilization buffers (eBioscience) were used as per the manufacturer's instructions to assess intracellular transcription factor and cytokine expression. Antibodies are listed in table S1.

T cell culture

Naive T cells were purified from the spleens and lymph nodes using the Naïve CD4$^+$ T Cell Isolation Kit according to the manufacturer's instructions (Miltenyi Biotec). Cells were cultured in Iscove's modified Dulbecco's medium (Sigma-Aldrich) and supplemented with 10% heat-inactivated FBS (Peak Serum), 50 U of penicillin-streptomycin (Life Technologies), 2 mM glutamine (Life Technologies), and 50 μM β-mercaptoethanol (Sigma-Aldrich). Naïve T cells were activated and differentiated in 24-well or 96-well plates precoated with rabbit anti-hamster IgG in the presence of anti-CD3ε (0.25 μg/ml; eBioscience), anti-CD28 (1 μg/ml; eBioscience), TGFβ (0.1 to 5.0 ng/ml; R&D Systems), and IL-6 (20 ng/ml; R&D Systems) for 48 to 72 hours.

The Jurkat human "T cell" line was maintained in RPMI 1640 medium (Gibco) supplemented with 10% FBS and 50 U of penicillin-streptomycin. Cells were cultured in the presence of vehicle [dimethyl sulfoxide (DMSO)] or DDX5 inhibitor RX-5902 (10 to 50 nM; ChemieTek). Cells were harvested 72 hours after treatment and analyzed by flow cytometry.

Retroviral transduction in T cells

sgRNAs were designed by CHOPCHOP (*48*) and cloned into the retroviral construct described previously by (*49*). sgRNA sequences are listed in table S2. PlatE cells were used to generate retrovirus as described in (*50*). Virus transduction in T cells was performed 24 hours after T cell activation by centrifugation at 2000 rpm for 90 min at 32°C. Live and CD90.1/Thy1.1$^+$-transduced cultured cells were analyzed by flow cytometry at 72 hours.

ChIP and DRIP

ChIP assays were performed on 5 to 10 million cultured T cells cross-linked with 1% formaldehyde. Chromatin was sonicated and immunoprecipitated using antibodies as listed in table S1 and Dynabeads (Thermo Fisher Scientific), followed by reverse cross-linking and genomic DNA purification. DRIP assays were performed on 5 to 8 million cells as described by (*51*). Briefly, cells were lysed, and chromatin DNA was fragmented. Anti–DNA-RNA hybrid antibodies (clone S9.6, Millipore) was used for immunoprecipitation (IP). qPCR primer sets are listed in table S2.

DDX5 eCLIP-seq

eCLIP-seq analysis was performed as previously described in (*52*) on UV cross-linked CTL-polarized T cells. Following cell lysis and treatment with ribonucleases (RNases), DDX5-containing RNA complexes were pulled down. RNA fragments protected from RNase digestion were subjected to RNA linker ligation, reverse transcription, and DNA linker ligation to generate eCLIP-seq libraries for high-throughput Illumina sequencing. Peaks were first defined using CLIPper on the IP sample (https://github.com/YeoLab/clipper/wiki/CLIPper-Home). Enrichments were calculated using both the IP and input samples. Log_2 fold change was calculated as eCLIP-seq reads normalized for read depth over normalized reads found at each peak region in the size-matched input sample. Significance tests were performed using Fisher's exact test or chi-square test, as described in (*52*). Encyclopedia of DNA Elements (ENCODE) irreproducible discovery rate analysis was performed on two independent biological replicates. Peaks were ranked using the entropy formula, $Pi\text{x}\log(Pi/Qi)/\log_2$, where Pi is the probability of an eCLIP-seq read at that position and Qi is the probability of input reads at that position. Results were filtered using cutoffs of 3 for both $\log_{10}$ P values and $\log_2$ fold changes to define a set of true peaks normalized above their respective size-matched input signal.

Protein and Western blot analysis

The NE-PER Kit (Thermo Fisher Scientific) was used for cytoplasmic and nuclear fractionation studies. Thirty to 50 μg of proteins were loaded on each lane. Blots were blocked in an Odyssey Blocking buffer (LICOR Biosciences) and probed with primary antibodies (table S1). Following incubation with respective IRDye secondary antibody (LICOR Biosciences), infrared signals on each blot were measured on the LICOR Odyssey CLX.

cDNA synthesis and qRT-PCR analysis

Total RNA was extracted with an RNeasy kit (QIAGEN) and reverse-transcribed using the iScript Select cDNA Synthesis Kit (Bio-Rad Laboratories). Real-time reverse transcription polymerase chain reaction (RT-PCR) was performed using iTaq Universal SYBR Green Supermix (Bio-Rad Laboratories). Expression data were normalized to *Gapdh* mRNA levels. Quantitative RT-PCR (qRT-PCR) primers were designed using Primer-BLAST to span across splice junctions, resulting in PCR amplicons that span at least one intron. Primer sequences are listed in table S2.

Statistical analysis

All values are presented as means ± SD. Significant differences were evaluated using GraphPad Prism 9 software. The Student's t tests or paired t tests were used to determine significant differences between the two groups. A two-tailed P value of <0.05 was considered statistically significant in all experiments.

Supplementary Materials

This PDF file includes:

Figs. S1 to S9

Tables S1 and S2

View/request a protocol for this paper from *Bio-protocol*.

REFERENCES AND NOTES

1. E. M. Shevach, Mechanisms of foxp3$^+$ T regulatory cell-mediated suppression. *Immunity* **30**, 636–645 (2009).
2. K. Pham, K. Parikh, E. C. Heinrich, Hypoxia and inflammation: Insights from high-altitude physiology. *Front. Physiol.* **12**, 676782 (2021).
3. C. T. Taylor, S. P. Colgan, Regulation of immunity and inflammation by hypoxia in immunological niches. *Nat. Rev. Immunol.* **17**, 774–785 (2017).
4. E. T. Clambey, E. McNamee, J. A. Westrich, L. E. Glover, E. L. Campbell, P. Jedlicka, E. F. de Zoeten, J. C. Cambier, K. R. Stenmark, S. P. Colgan, H. K. Eltzschig, Hypoxia-inducible factor-1α-dependent induction of FoxP3 drives regulatory T-cell abundance and function during inflammatory hypoxia of the mucosa. *Proc. Natl. Acad. Sci. U.S.A.* **109**, E2784–E2793 (2012).
5. E. V. Dang, J. Barbi, H.-Y. Yang, D. Jinasena, H. Yu, Y. Zheng, Z. Bordman, J. Fu, Y. Kim, H.-R. Yen, W. Luo, K. Zeller, L. Shimoda, S. L. Topalian, G. L. Semenza, C. V. Dang, D. M. Pardoll, F. Pan, Control of T_H17/T_{reg} balance by hypoxia-inducible factor 1. *Cell* **146**, 772–784 (2011).
6. L. Z. Shi, R. Wang, G. Huang, P. Vogel, G. Neale, D. R. Green, H. Chi, HIF1α–dependent glycolytic pathway orchestrates a metabolic checkpoint for the differentiation of T_H17 and T_{reg} cells. *J. Exp. Med.* **208**, 1367–1376 (2011).
7. W. J. Yang, H. Liu, L. Xu, T. Yu, X. Zhao, S. Yao, Q. Zhao, S. Barnes, S. M. Cohn, S. M. Dann, H. Zhang, X. Zuo, Y. Li, Y. Cong, GPR120 inhibits colitis through regulation of CD4$^+$ T cell interleukin 10 production. *Gastroenterology* **162**, 150–165 (2022).
8. E. Sefik, N. Geva-Zatorsky, S. Oh, L. Konnikova, D. Zemmour, A. M. McGuire, D. Burzyn, A. Ortiz-Lopez, M. Lobera, J. Yang, S. Ghosh, A. Earl, S. B. Snapper, R. Jupp, D. Kasper, D. Mathis, C. Benoist, Individual intestinal symbionts induce a distinct population of RORγ$^+$ regulatory T cells. *Science* **349**, 993–997 (2015).
9. M. Xu, M. Pokrovskii, Y. Ding, R. Yi, C. Au, O. J. Harrison, C. Galan, Y. Belkaid, R. Bonneau, D. R. Littman, c-MAF-dependent regulatory T cells mediate immunological tolerance to a gut pathobiont. *Nature* **554**, 373–377 (2018).
10. B. H. Yang, S. Hagemann, P. Mamareli, U. Lauer, U. Hoffmann, M. Beckstette, L. Föhse, I. Prinz, J. Pezoldt, S. Suerbaum, T. Sparwasser, A. Hamann, S. Floess, J. Huehn, M. Lochner, Foxp3$^+$ T cells expressing RORγt represent a stable regulatory T-cell effector lineage with enhanced suppressive capacity during intestinal inflammation. *Mucosal Immunol.* **9**, 444–457 (2016).
11. B. S. Kim, H. Lu, K. Ichiyama, X. Chen, Y.-B. Zhang, N. A. Mistry, K. Tanaka, Y.-h. Lee, R. Nurieva, L. Zhang, X. Yang, Y. Chung, W. Jin, S. H. Chang, C. Dong, Generation of RORγt$^+$ antigen-specific T regulatory 17 cells from Foxp3$^+$ precursors in autoimmunity. *Cell Rep.* **21**, 195–207 (2017).
12. T. Long, N. Abbasi, J. E. Hernandez, Y. Li, I. M. Sayed, S. Ma, A. Iemolo, B. A. Yee, G. W. Yeo, F. Telese, P. Ghosh, S. Das, W. J. M. Huang, RNA binding protein DDX5 directs tuft cell specification and function to regulate microbial repertoire and disease susceptibility in the intestine. *Gut* **71**, 1790–1802 (2022).
13. C. F. Bourgeois, F. Mortreux, D. Auboeuf, The multiple functions of RNA helicases as drivers and regulators of gene expression. *Nat. Rev. Mol. Cell Biol.* **17**, 426–438 (2016).

14. G. Giraud, S. Terrone, C. F. Bourgeois, Functions of DEAD box RNA helicases DDX5 and DDX17 in chromatin organization and transcriptional regulation. *BMB Rep.* **51**, 613–622 (2018).
15. F. V. Fuller-Pace, The DEAD box proteins DDX5 (p68) and DDX17 (p72): Multi-tasking transcriptional regulators. *Biochim. Biophys. Acta* **1829**, 756–763 (2013).
16. Z. Wang, Z. Luo, L. Zhou, X. Li, T. Jiang, E. Fu, DDX5 promotes proliferation and tumorigenesis of non-small-cell lung cancer cells by activating β-catenin signaling pathway. *Cancer Sci.* **106**, 1303–1312 (2015).
17. A. Mazurek, Y. Park, C. Miething, J. E. Wilkinson, J. Gillis, S. W. Lowe, C. R. Vakoc, B. Stillman, Acquired dependence of acute myeloid leukemia on the DEAD-box RNA helicase DDX5. *Cell Rep.* **7**, 1887–1899 (2014).
18. Z. Yu, S. Y. Mersaoui, L. Guitton-Sert, Y. Coulombe, J. Song, J.-Y. Masson, S. Richard, DDX5 resolves R-loops at DNA double-strand breaks to promote DNA repair and avoid chromosomal deletions. *NAR Cancer* **2**, zcaa028 (2020).
19. O. D. Villarreal, S. Y. Mersaoui, Z. Yu, J. Y. Masson, S. Richard, Genome-wide R-loop analysis defines unique roles for DDX5, XRN2, and PRMT5 in DNA/RNA hybrid resolution. *Life Sci. Alliance* **3**, e202000762 (2020).
20. S. Y. Mersaoui, Z. Yu, Y. Coulombe, M. Karam, F. F. Busatto, J.-Y. Masson, S. Richard, Arginine methylation of the DDX5 helicase RGG/RG motif by PRMT5 regulates resolution of RNA:DNA hybrids. *EMBO J.* **38**, e100986 (2019).
21. Y. Li, Y. Song, W. Xu, Q. Li, X. Wang, K. Li, J. Wang, Z. Liu, S. Velychko, R. Ye, Q. Xia, L. Wang, R. Guo, X. Dong, Z. Zheng, Y. Dai, H. Li, M. Yao, Y. Xue, H. R. Schöler, Q. Sun, H. Yao, R-loops coordinate with SOX2 in regulating reprogramming to pluripotency. *Sci. Adv.* **6**, eaba0777 (2020).
22. G. Sessa, B. Gómez-González, S. Silva, C. Pérez-Calero, R. Beaurepere, S. Barroso, S. Martineau, C. Martin, Å. Ehlén, J. S. Martínez, B. Lombard, D. Loew, S. Vagner, A. Aguilera, A. Carreira, BRCA2 promotes DNA-RNA hybrid resolution by DDX5 helicase at DNA breaks to facilitate their repair‡. *EMBO J.* **40**, e106018 (2021).
23. K. Skourti-Stathaki, K. Kamieniarz-Gdula, N. J. Proudfoot, R-loops induce repressive chromatin marks over mammalian gene terminators. *Nature* **516**, 436–439 (2014).
24. D. Y. Zhao, G. Gish, U. Braunschweig, Y. Li, Z. Ni, F. W. Schmitges, G. Zhong, K. Liu, W. Li, J. Moffat, M. Vedadi, J. Min, T. J. Pawson, B. J. Blencowe, J. F. Greenblatt, SMN and symmetric arginine dimethylation of RNA polymerase II C-terminal domain control termination. *Nature* **529**, 48–53 (2016).
25. N. Abbasi, T. Long, Y. Li, B. A. Yee, B. S. Cho, J. E. Hernandez, E. Ma, P. R. Patel, D. Sahoo, I. M. Sayed, N. Varki, S. das, P. Ghosh, G. W. Yeo, W. J. M. Huang, DDX5 promotes oncogene C3 and FABP1 expressions and drives intestinal inflammation and tumorigenesis. *Life Sci. Alliance* **3**, e202000772 (2020).
26. W. Ouyang, A. O'Garra, IL-10 family cytokines IL-10 and IL-22: From basic science to clinical translation. *Immunity* **50**, 871–891 (2019).
27. M. Friedrich, M. Pohin, F. Powrie, Cytokine networks in the pathophysiology of inflammatory bowel disease. *Immunity* **50**, 992–1006 (2019).
28. S. Lin, L. Tian, H. Shen, Y. Gu, J. L. Li, Z. Chen, X. Sun, M. James You, L. Wu, DDX5 is a positive regulator of oncogenic NOTCH1 signaling in T cell acute lymphoblastic leukemia. *Oncogene* **32**, 4845–4853 (2013).
29. S. Ma, S. A. Patel, Y. Abe, N. Chen, P. R. Patel, B. S. Cho, N. Abbasi, S. Zeng, B. Schnabl, J. T. Chang, W. J. M. Huang, RORγt phosphorylation protects against T cell-mediated inflammation. *Cell Rep.* **38**, 110520 (2022).
30. S. Ma, J. E. Hernandez, W. J. M. Huang, Protocol to assess cell-intrinsic regulatory mechanisms using an ex vivo murine T cell polarization and co-culture system. *STAR Protoc.* **3**, 101543 (2022).
31. Y. J. Lee, Q. Wang, D. C. Rio, Coordinate regulation of alternative pre-mRNA splicing events by the human RNA chaperone proteins hnRNPA1 and DDX5. *Genes Dev.* **32**, 1060–1074 (2018).
32. V. Hashemi, A. Ahmadi, F. Malakotikhah, M. G. Chaleshtari, M. Baghi Moornani, A. Masjedi, M. Sojoodi, F. Atyabi, A. Nikkhoo, N. Rostami, B. Baradaran, G. Azizi, B. Yousefi, G. Ghalamfarsa, F. Jadidi-Niaragh, Silencing of p68 and STAT3 synergistically diminishes cancer progression. *Life Sci.* **249**, 117499 (2020).
33. H. Shehade, V. Acolty, M. Moser, G. Oldenhove, Cutting edge: Hypoxia-inducible factor 1 negatively regulates T_H1 function. *J. Immunol.* **195**, 1372–1376 (2015).
34. S. G. Manzo, S. R. Hartono, L. A. Sanz, J. Marinello, S. de Biasi, A. Cossarizza, G. Capranico, F. Chedin, DNA topoisomerase I differentially modulates R-loops across the human genome. *Genome Biol.* **19**, 100 (2018).
35. K. Arab, E. Karaulanov, M. Musheev, P. Trnka, A. Schäfer, I. Grummt, C. Niehrs, GADD45A binds R-loops and recruits TET1 to CpG island promoters. *Nat. Genet.* **51**, 217–223 (2019).
36. L. Chen, J.-Y. Chen, X. Zhang, Y. Gu, R. Xiao, C. Shao, P. Tang, H. Qian, D. Luo, H. Li, Y. Zhou, D.-E. Zhang, X.-D. Fu, R-ChIP using Inactive RNase H reveals dynamic coupling of R-loops with transcriptional pausing at gene promoters. *Mol. Cell* **68**, 745–757.e5 (2017).
37. M. P. Crossley, M. Bocek, K. A. Cimprich, R-Loops as cellular regulators and genomic threats. *Mol. Cell* **73**, 398–411 (2019).
38. G. C. Kost, M. Y. Yang, L. Li, Y. Zhang, C. Y. Liu, D. J. Kim, C. H. Ahn, Y. B. Lee, Z. R. Liu, A novel anti-cancer agent, 1-(3,5-dimethoxyphenyl)-4-[(6-fluoro-2-methoxyquinoxalin-3-yl)aminocarbonyl] piperazine (RX-5902), interferes with β-catenin function through Y593 phospho-p68 RNA helicase. *J. Cell. Biochem.* **116**, 1595–1601 (2015).
39. P. Zhou, C. Streutker, R. Borojevic, Y. Wang, K. Croitoru, IL-10 modulates intestinal damage and epithelial cell apoptosis in T cell-mediated enteropathy. *Am. J. Physiol. Gastrointest. Liver Physiol.* **287**, G599–G604 (2004).
40. S. Huber, N. Gagliani, E. Esplugues, W. O'Connor Jr., F. J. Huber, A. Chaudhry, M. Kamanaka, Y. Kobayashi, C. J. Booth, A. Y. Rudensky, M. G. Roncarolo, M. Battaglia, R. A. Flavell, T_H17 cells express interleukin-10 receptor and are controlled by $Foxp3^-$ and $Foxp3^+$ regulatory $CD4^+$ T cells in an interleukin-10-dependent manner. *Immunity* **34**, 554–565 (2011).
41. L. M. M. Costes, D. J. Lindenbergh-Kortleve, L. A. van Berkel, S. Veenbergen, H. R. C. Raatgeep, Y. Simons-Oosterhuis, D. H. van Haaften, J. J. Karrich, J. C. Escher, M. Groeneweg, B. E. Clausen, T. Cupedo, J. N. Samsom, IL-10 signaling prevents gluten-dependent intraepithelial $CD4^+$ cytotoxic T lymphocyte infiltration and epithelial damage in the small intestine. *Mucosal Immunol.* **12**, 479–490 (2019).
42. G. Nizzoli, C. Burrello, F. M. Cribiù, G. Lovati, G. Ercoli, F. Botti, E. Trombetta, L. Porretti, K. Todoerti, A. Neri, M. R. Giuffrè, J. Geginat, M. Vecchi, M. Rescigno, M. Paroni, F. Caprioli, F. Facciotti, Pathogenicity of In Vivo Generated Intestinal Th17 Lymphocytes is IFNγ Dependent. *J. Crohns Colitis* **12**, 981–992 (2018).
43. K. K. Chang, L. B. Liu, L. P. Jin, B. Zhang, J. Mei, H. Li, C. Y. Wei, W. J. Zhou, X. Y. Zhu, J. Shao, D. J. Li, M. Q. Li, IL-27 triggers IL-10 production in Th17 cells via a c-Maf/RORγt/Blimp-1 signal to promote the progression of endometriosis. *Cell Death Dis.* **8**, e2666 (2017).
44. C. Asseman, S. Mauze, M. W. Leach, R. L. Coffman, F. Powrie, An essential role for interleukin 10 in the function of regulatory T cells that inhibit intestinal inflammation. *J. Exp. Med.* **190**, 995–1004 (1999).
45. X. Wu, A. Lahiri, G. K. Haines III, R. A. Flavell, C. Abraham, NOD2 regulates CXCR3-dependent $CD8^+$ T cell accumulation in intestinal tissues with acute injury. *J. Immunol.* **192**, 3409–3418 (2014).
46. S. M. Nicol, S. E. Bray, H. D. Black, S. A. Lorimore, E. G. Wright, D. P. Lane, D. W. Meek, P. J. Coates, F. V. Fuller-Pace, The RNA helicase p68 (DDX5) is selectively required for the induction of p53-dependent p21 expression and cell-cycle arrest after DNA damage. *Oncogene* **32**, 3461–3469 (2013).
47. L. Lefrancois, N. Lycke, Isolation of mouse small intestinal intraepithelial lymphocytes, Peyer's patch, and lamina propria cells. *Curr. Protoc. Immunol.* **Chapter 3**, Unit 3.19 (2001).
48. K. Labun, T. G. Montague, M. Krause, Y. N. Torres Cleuren, H. Tjeldnes, E. Valen, CHOPCHOP v3: Expanding the CRISPR web toolbox beyond genome editing. *Nucleic Acids Res.* **47**, W171–W174 (2019).
49. F. A. Ran, P. D. Hsu, J. Wright, V. Agarwala, D. A. Scott, F. Zhang, Genome engineering using the CRISPR-Cas9 system. *Nat. Protoc.* **8**, 2281–2308 (2013).
50. S. Morita, T. Kojima, T. Kitamura, Plat-E: an efficient and stable system for transient packaging of retroviruses. *Gene Ther.* **7**, 1063–1066 (2000).
51. L. A. Sanz, F. Chedin, High-resolution, strand-specific R-loop mapping via S9.6-based DNA-RNA immunoprecipitation and high-throughput sequencing. *Nat Protoc* **14**, 1734–1755 (2019).
52. E. L. Van Nostrand, G. A. Pratt, A. A. Shishkin, C. Gelboin-Burkhart, M. Y. Fang, B. Sundararaman, S. M. Blue, T. B. Nguyen, C. Surka, K. Elkins, R. Stanton, F. Rigo, M. Guttman, G. W. Yeo, Robust transcriptome-wide discovery of RNA-binding protein binding sites with enhanced CLIP (eCLIP). *Nat. Methods* **13**, 508–514 (2016).
53. J. C. Martin, C. Chang, G. Boschetti, R. Ungaro, M. Giri, J. A. Grout, K. Gettler, L.-S. Chuang, S. Nayar, A. J. Greenstein, M. Dubinsky, L. Walker, A. Leader, J. S. Fine, C. E. Whitehurst, M. L. Mbow, S. Kugathasan, L. A. Denson, J. S. Hyams, J. R. Friedman, P. T. Desai, H. M. Ko, I. Laface, G. Akturk, E. E. Schadt, H. Salmon, S. Gnjatic, A. H. Rahman, M. Merad, J. H. Cho, E. Kenigsberg, Single-cell Analysis of Crohn's disease lesions identifies a pathogenic cellular module associated with resistance to anti-TNF therapy. *Cell* **178**, 1493–1508.e20 (2019).
54. J. C. Devlin, J. Axelrad, A. M. Hine, S. Chang, S. Sarkar, J. D. Lin, K. V. Ruggles, D. Hudesman, K. Cadwell, P. Loke, Single-cell transcriptional survey of ileal-anal pouch immune cells from ulcerative colitis patients. *Gastroenterology* **160**, 1679–1693 (2021).

Acknowledgments: We thank F. Fuller-Pace at the University of Dundee for sharing the DDX5 conditional mutant mice previously described in (*1*). We thank J. Zuber and A. Martin at the Research Institute of Molecular Pathology (I.M.P.) for sharing the pSIN vector for generating retroviruses to carry custom sgRNAs into T cells. **Funding:** This work was supported by the Edward Mallinckrodt Jr. Foundation (to W.J.M.H.); the NIH grants R01-GM124494 (to W.J.M.H.), R01-HG004659 and U41-HG009889 (to G.W.Y.), S10-OD026929, and P30-CA023100; the NOMIS fellowship (to Q.Y.); the NIH grants R01-AI107027, R01-AI1511123, R21-AI154919, and P30-CA014195 (to Y.Z.); the NOMIS Foundation (to Y.Z.); the NIH grant R00-DK110534 (to H.C.); and

the Chiba University–UC San Diego Center for Mucosal Immunology, Allergy and Vaccines (to H.C.). **Author contributions:** Conceptualization: S.M. and W.J.M.H.. Methodology: S.M., Q.Y., N.A., and B.A.Y. Investigation: S.M., Q.Y., N.C., A.Z., P.R.P., B.S.C., L.Z., and G.W. Visualization: S.M., N.C., and W.J.M.H. Funding acquisition: W.J.M.H., G.W.Y., Y.Z., and H.C. Project administration: W.J.M.H. Supervision: W.J.M.H., Y.Z., G.W.Y., S.M.E., and H.C. Writing—original draft: S.M. and W.J.M.H. Writing–review and editing: W.J.M.H., S.M., S.M.E., and G.W.Y. **Competing interests:** G.W. Yeo is cofounder, member of the board of directors, scientific advisory board, equity holder, and paid consultant for Locanabio and Eclipse BioInnovations. G.W.Y. is a visiting professor at the National University of Singapore. G.W.Y.'s interests have been reviewed and approved by the University of California San Diego in accordance with its conflict of interest policies. All other authors declare that they have no competing interests. **Data and materials availability:** All data needed to evaluate the conclusions in the paper are present in the paper and/or the Supplementary Materials. Raw sequencing data for the eCLIP-seq experiment are available at Gene Expression Omnibus (GEO) under accession number GSE157259.

Submitted 22 June 2022
Accepted 5 January 2023
Published 1 February 2023
10.1126/sciadv.add6165